3-2020

Biomimetic Metal-Organic Nanoparticles Prepared with a 3D-Printed Microfluidic Device as a Novel Formulation for Disulfiram-Based Therapy Against Breast Cancer

Ya Chang

Jizong Jiang

Wu Chen

Wen Yang

Lili Chen

See next page for additional authors

Authors

Ya Chang, Jizong Jiang, Wu Chen, Wen Yang, Lili Chen, Pengyu Chen, Jianzhong Shen, Shizhi Qian, Teng Zhou, Linfeng Wu, Liang Hong, Yongzhuo Huang, and Feng Li

Applied Materials Today 18 (2020) 100492

Contents lists available at ScienceDirect

Applied Materials Today

journal homepage: www.elsevier.com/locate/apmt

Biomimetic metal-organic nanoparticles prepared with a 3D-printed microfluidic device as a novel formulation for disulfiram-based therapy against breast cancer

Ya Chang[a,1], Jizong Jiang[b,1], Wu Chen[a], Wen Yang[c], Lili Chen[c], Pengyu Chen[c], Jianzhong Shen[a], Shizhi Qian[d], Teng Zhou[d], Linfeng Wu[e], Liang Hong[e], Yongzhuo Huang[b,**], Feng Li[a,*]

[a] Department of Drug Discovery and Development, Harrison School of Pharmacy, Auburn University, Auburn, AL, 36849, USA
[b] State Key Laboratory of Drug Research, Shanghai Institute of Materia Medica, Chinese Academy of Sciences, Shanghai, 201203, China
[c] Materials Research and Education Center, Materials Engineering, Department of Mechanical Engineering, Auburn University, Auburn, AL, 36849, USA
[d] Department of Mechanical and Aerospace Engineering, Old Dominion University, Norfolk, VA, 23529, USA
[e] College of Dentistry, University of Tennessee Health Science Center, Memphis, TN, 38163, USA

ARTICLE INFO

Article history:
Received 2 August 2019
Received in revised form
24 September 2019
Accepted 20 October 2019

Keywords:
Biomimetic delivery
Metal-organic nanoparticle
Disulfiram
Copper diethyldithiocarbamate
Microfluidic
Breast cancer

ABSTRACT

Disulfiram (DSF) is currently tested in several clinical trials for cancer treatment in combination with copper (Cu) ions. Usually, DSF and Cu are administered in two separate formulations. In the body, DSF and Cu ions form diethyldithiocarbamate copper complex [$Cu(DDC)_2$] which has potent antitumor activities. However, the "two formulation" approach often achieved low $Cu(DDC)_2$ concentration at tumor regions and resulted in compromised anticancer efficacy. Therefore, preformed $Cu(DDC)_2$ complex administered in a single formulation will have better anticancer efficacy. However, the poor aqueous solubility of $Cu(DDC)_2$ is a significant challenge for its clinical use. In this work, a biomimetic nanoparticle formulation of $Cu(DDC)_2$ was produced with a novel **SMILE** (**S**tabilized **M**etal **I**on **L**igand compl**e**x) method developed in our laboratory to address the drug delivery challenges. The Metal-organic Nanoparticle (MON) is composed of $Cu(DDC)_2$ metal-organic complex core and surface decorated bovine serum albumin (BSA). Importantly, we designed a 3D-printed microfluidic device to further improve the fabrication of BSA/$Cu(DDC)_2$ MONs. This method could precisely control the MON preparation process and also has great potential for large scale production of $Cu(DDC)_2$ MON formulations. We also used a computational modeling approach to simulate the MON formation process in the microfluidic device. The optimized BSA/$Cu(DDC)_2$ MONs demonstrated good physicochemical properties. The MONs also showed potent antitumor activities in the breast cancer cell monolayers as well as the 3D-cultured tumor spheroids. The BSA/$Cu(DDC)_2$ MONs also effectively inhibited the growth of tumors in an *orthotopic* 4T1 breast tumor model. This current study provided a novel method to prepare a biomimetic MON formulation for DSF/Cu cancer therapy.

1. Introduction

Disulfiram (DSF) has been approved by the FDA for treating alcohol abuse for more than six decades. Recently, DSF was repurposed for cancer treatment due to its anticancer activities. Drug repurposing is a promising approach for drug discovery and development [1], which could shorten the development course, reduce the risk of failure, and save R&D costs. DSF monotherapy only demonstrated limited efficacy, while the combination of DSF and copper ions (Cu^{2+}) showed significantly enhanced anticancer activities [2,3]. Diethyldithiocarbamate (a DSF metabolite) could complex with Cu^{2+} ions and generate diethyldithiocarbamate copper [$Cu(DDC)_2$] which is a key player that accounts for the antitumor efficacy of DSF/Cu combination therapy [4]. In many studies including clinical trials, DSF and Cu^{2+} were co-administered in separate formulations (www.clinicaltrials.gov). DSF is rapidly metabolized and degraded in the body [3,5]. Therefore, co-administration of DSF and Cu^{2+} in two separate formulations usually yielded a very low concentration of the active ingredient, $Cu(DDC)_2$, in the tumor region and resulted in only marginal anticancer efficacy. Therefore, the delivery of preformed $Cu(DDC)_2$ in a single formulation is a more effective method to achieve a higher $Cu(DDC)_2$ concentration in tumor and improve the anticancer efficacy [6].

* Corresponding author at: 720 S. Donahue Dr. Auburn, AL, 36849, USA.
** Corresponding author at: 501 Haike Rd., Shanghai, 201203, China.
E-mail addresses: yzhuang@simm.ac.cn (Y. Huang), FZL0023@auburn.edu (F. Li).
[1] Equal contribution.

https://doi.org/10.1016/j.apmt.2019.100492
2352-9407/

However, the poor aqueous solubility of $Cu(DDC)_2$ complex created a formidable hurdle for its clinical use. Several different nanomedicine formulations (*e.g.,* solid nanoparticle, liposome, and micelle) were used to deliver $Cu(DDC)_2$ and achieved improved efficacy [6–9]. Yet, there still are some challenges to be overcome: (1) the complicated preparation processes are incompatible with large-scale production; and (2) many formulations only achieved low drug concentrations and were hard to obtain the minimal drug concentration for clinical use. Due to the lack of appropriate formulations, the clinical application of this drug is very limited. There is a great need for developing a formulation that is suitable for clinical use.

In our previous study, we developed a **Stabilized Metal Ion Ligand Nanocomplex** (**SMILE**) technology to prepare $Cu(DDC)_2$ metal-organic nanoparticles (MONs). And methoxy poly(ethylene glycol)$_{5000}$-*b*-poly(L-lactide)$_{5000}$ (PEG-PLA) was used as the stabilizer [10]. The SMILE method can achieve superior yield and high drug concentration; requires a simple formulation and preparation process; and has excellent formulation properties. In this work, we will prepare biomimetic albumin-decorated $Cu(DDC)_2$ MONs with the SMILE technology. In addition, we further improved the SMILE technology by using a 3D-printed microfluidic device for scalable continuous production of $Cu(DDC)_2$ MONs. With the aid of the microfluidic device, we could achieve precise control of the mixing process, easily scale up the preparation process for mass production, and thus facilitate the clinical translation and future commercialization.

2. Materials and methods

2.1. Materials

Most chemicals and supplies used in this study were purchased from VWR International (Radnor, USA). D-α-Tocopherol polyethylene glycol 1000 succinate (TPGS) was ordered from Sigma-Aldrich and used without purification (St. Louis, USA). Cyanine5 NHS ester was obtained from Dalian Meilun Biotechnology Co., Ltd (Dalian, China).

2.2. Production of $Cu(DDC)_2$ MONs with the SMILE method

2.2.1. Vortexing method

The vortexing method of preparing $Cu(DDC)_2$ MONs was described in our previous paper [10]. Briefly, copper chloride ($CuCl_2$) and sodium diethyldithiocarbamatetrihydrate (DDC-Na) were dissolved with two BSA containing aqueous solutions, respectively. Then, these two solutions were vigorously mixed by vortexing at a molar ratio of 2:1 (DDC-Na *vs* $CuCl_2$). The $Cu(DDC)_2$ MONs formed by DDC-Na and $CuCl_2$ were stabilized by BSA. Large aggregations were removed by centrifugation for 10 min at 6700 *g* and followed by filtration with a 0.45 μm filter. The influence of $CuCl_2$, DDC-Na, and BSA concentration was extensively investigated.

2.2.2. Microfluidic device method

We first prepared a microfluidic mixing device with a 3D printer (Fig. S1). The device was printed with a HICTOP Creality CR-10 3D-printer using PLA as the printing material. Then, the DDC-Na solution and $CuCl_2$ solution were delivered into the mixing device through two inlets with syringe pumps (Fig. 3A). The resulting MONs were collected from the outlet and purified by centrifugation and filtration with the same procedure as described in the vortexing method.

2.3. Determination of particle size, zeta potential, and morphology

2.3.1. Particle size and zeta potential

The particle size and polydispersity index (PDI) were determined with Malvern Nano ZS based on the dynamic light scattering [11]. The MONs were diluted with water before measurement. The particle size and PDI were determined at 173-degree scattering angle. The zeta potential was also determined with the Malvern Nano ZS.

2.3.2. Transmission Electron Microscope (TEM)

To characterize the MONs with TEM, samples were first added onto a grid and followed by uranyl acetate staining [12,13]. Then, samples were observed under a JEOL 2000EX Transmission Electron Microscope (Tokyo, Japan).

2.4. Determine drug concentration and yield

Drug concentrations in NP formulations were determined with the UV–vis spectrophotometric assay. Briefly, formulations were dissolved in dimethylformamide (DMF). The concentration of $Cu(DDC)_2$ was determined by the absorbance at 435 nm and calculated with the standard solution of $Cu(DDC)_2$ dissolved in DMF. The yield was calculated with this equation:

$$Yield\ (\%) = (Actual\ \ Drug\ \ Concentration\ /Theoretical\ \ Drug\ \ Concentration)\ \times\ 100\% \quad (1)$$

2.5. Stability

To determine the influence of serum on stability, the MON formulations were mixed with fetal bovine serum (FBS) solution (10% w/v) and incubated at a temperature of 37 °C. Then, at different time points, the particle size and PDI were measured. To determine long-term storage stability, the MON formulations were stored at room temperature (25 °C) or refrigerator (4 °C). $Cu(DDC)_2$ concentrations were determined at different days.

2.6. Modeling of MON formation process in the microfluidic device

The fluid within the microfluidic device is incompressible Newtonian fluid, and we further assume that the fluid properties such as density and viscosity are constants and independent of the concentration of the formed MONs. Under steady-state, the flow is described by the Navier–Stokes equations and the continuity equation:

$$\rho(\mathbf{u}\cdot\nabla)\mathbf{u} = -\nabla p + \nabla\cdot\eta(\nabla\mathbf{u} + (\nabla\mathbf{u})^T), \quad (2)$$

$$\nabla\cdot\mathbf{u} = 0. \quad (3)$$

In the above, **u** is the fluid velocity, p is the fluid pressure, η and ρ are, respectively, viscosity and density of the fluid.

The concentrations of the species, DDC-Na, $CuCl_2$, and the formed $Cu(DDC)_2$ MONs are described by the time-dependent convection-diffusion-reaction equations:

$$\frac{\partial c_i}{\partial t} + \mathbf{u}\cdot\nabla c_i = D_i\nabla^2 c_i + R_i, \quad (4)$$

Where c_i, D_i and R_i are, respectively, the molar concentration, diffusion coefficient, and rate of reaction of the i^{th} species (i = 1 for DDC-Na, 2 for $CuCl_2$, and 3 for $Cu(DDC)_2$). The reaction rates of the

irreversible chemical reactions 2 DDC-Na + $CuCl_2 \rightarrow Cu(DDC)_2$ + 2 $NaCl_2$ are given by:

$$R_1 = R_2 = -R_3 = -kc_1c_2, \quad (5)$$

with the rate constant, *k*, determined based on the Arrhenius equation.

For the steady-state Navier-Stokes equations, constant flow rates of 0.5, 1, and 2 mL/min, respectively, were imposed at the two inlets. Non-slip boundary condition (*i.e.*, $\mathbf{u} = \mathbf{0}$) was imposed on the solid microfluidic channel wall, and outflow with pressure p = 0 was applied at the outlet.

For the time-dependent convection-diffusion equations, the concentrations of $CuCl_2$ and DDC-Na of the two inlets were 11 mmol/L and 22 mmol/L, respectively, and the other rigid boundaries were non-flux boundaries. At the outlet, $\mathbf{n} \cdot D_i \nabla c_i = 0$ was set for the concentration of the ith species. At time = 0, the initial condition for each species within the microfluidic channel has zero concentration. In this study, we set the density $\rho = 2000\,kg/m^3$, dynamic viscosity $\mu = 0.001\,Pa \cdot s$, diffusion coefficients the ith (i = 1,2 and 3) species are, respectively, $1 \times 10^{-9}\,m^2/s$, $1 \times 10^{-9}\,m^2/s$, and $1 \times 10^{-10}\,m^2/s$. We first solve the steady-state Navier Stokes equations by using the commercial finite element package, Comsol (www.comsol.com), installed in a high-performance cluster. With the known flow field, we solve the time-dependent convection-diffusion-reaction equations for the concentrations of the species.

2.7. MTT assay

4T1 mouse breast cancer cells were obtained from the American Type Culture Collection (ATCC). The culture medium was Roswell Park Memorial Institute (RPMI) 1640 containing 1% Antibiotic-Antimycotic and 10% FBS. MD Anderson-Metastatic Breast-231 (MDA-MB-231) cells (ATCC) were cultured with a mixture of Ham's F-12 Medium and Dulbecco's Modified Eagle's Medium (DMEM) (1:1) containing 1% Antibiotic-Antimycotic and 10% FBS. Cells were cultured in a humidified incubator with 5% CO_2 at 37 °C.

To test cytotoxicity, cells were seeded into a 96-well plate (5000 cells/well) and incubated overnight to allow cells to attach to the plate. Then, different test agents with various concentrations were diluted with cell culture medium and added into wells (100 μL/well). At the end of treatment, cytotoxicity was determined with 3-(4,5-dimethyl-thiazol-2-yl)-2, 5-diphenyl tetrazolium bromide (MTT) assay [12,14–17]. The absorbance was determined at 570 nm and subtracted by the reference absorbance at 670 nm. The following equation was used to calculate the cell viability:

$$\text{Cell Viability}(\%) = (A_{Test}/A_{control}) \times 100\%$$

GraphPad Prism software was used to calculate the IC_{50}.

2.8. Calcein-AM/Propidium Iodide (PI) staining

Cells were added into a 96-well plate at a density of 10,000 cells/well one night before experiment. Then, cells were treated for 24 h with different formulations and followed by Calcein-AM and PI staining. The staining solution was prepared by diluting Calcein-AM and PI stock solutions in pH 7.4 phosphate-buffered saline (PBS). Both dead cells with red fluorescence and viable cells with green fluorescence will be analyzed with the Cytation 5 Cell Imaging Multi-Mode Reader.

2.9. Penetration and cytotoxicity on tumor cell spheroids

Tumor spheroids were established with a liquid overlay method [18]. Briefly, 4T1 cells were seeded in a 96-well plate pretreated with agarose gel (1% w/v). After 7 days of culture, spheroids were treated with various testing formulations for 72 h. The morphology of spheroids was recorded with microscopy. The cytotoxicity was determined with the Calcein-AM/Propidium Iodide (PI) staining method as well as CellTiter-Blue reagents (Promega). For the Calcein-AM/Propidium Iodide (PI), tumor spheroids were incubated with a staining solution containing PI (3μM) and Calcein-AM (3μM) in pH 7.4 phosphate-buffered saline (PBS) at 37 °C for 30 min. Both dead cells with red fluorescence and viable cells with green fluorescence will be analyzed with the Cytation 5 Cell Imaging Multi-Mode Reader. For the CellTiter-Blue reagent assay, the CellTiter-Blue reagents were mixed with treated tumor spheroids and incubated for 24 h. At the end of incubation, the fluorescence intensity was determined with the Cytation 5 Cell Imaging Multi-Mode Reader ($EX_{560\,nm}$ and $EM_{590\,nm}$). To determine penetration ability of the nanoparticles in tumor spheroids, cyanine 5 (Cy5)-labeled BSA $Cu(DDC)_2$ MONs were synthesized as previously reported [7] and incubated with tumor spheroids for 3 h at 37 °C. At the end of incubation, spheroids were then rinsed with PBS three times and analyzed with confocal microscopy (TCS-SP8, Leica, Germany).

2.10. Would healing study

The 4T1 or MDA-MB-231 cells were seeded at a 96-well plate at a density of 10,000 cells/well and cultured at 37 °C overnight before test. Scratch on the cell monolayer was created with a 10 μL pipette tip. Then, cells were treated with different formulations for 18 h. Cell migration distance was determined by comparing the scratch width at the end of treatment with the initial scratch width.

2.11. In vivo *orthotopic breast tumor model, biodistribution, and anticancer efficacy study*

Balb/c mice (female, 4 weeks) were purchased from the Shanghai Laboratory Animal Center (SLAC) Co., Ltd. (Shanghai, China). Animals were housed at the SPF care facility under a 12 h light/dark cycle with distilled water and sterilized food pellets. Animal study protocols were approved by the Institutional Animal Care and Use Committee (IACUC) of SIMM and performed in accordance with the Guidelines for Care and Use of Laboratory Animals of Shanghai Institute of Materia Medica (SIMM), Chinese Academy of Sciences. The animal models with orthotopic breast tumors were established by injecting 4T1 cells (1×10^6 cells) into the second mammary fat pad of the Balb/c mice [18]. Treatments were initiated when the tumors were reached an average volume of 80–90 mm^3. Tumor size (mm^3) = [width (mm)^2 × length (mm)] × 1/2. Mice were randomly divided into six groups (5 mice per group) and received intravenous administration of $Cu(DDC)_2$ solution containing 10% (2-Hydroxypropyl)-β-cyclodextrin and 5% ethanol (3 mg/Kg $Cu(DDC)_2$), BSA $Cu(DDC)_2$ MONs (1.5 mg/Kg $Cu(DDC)_2$), and BSA $Cu(DDC)_2$ MONs (3 mg/Kg $Cu(DDC)_2$), and equivalent dose of BSA, $CuCl_2$ aqueous solution, DDC-Na aqueous solution. Mice received a total of three treatments on day 7, 10, and 13, respectively. Body weight and tumor volume were monitored and recorded. At the end of the experiment, the mice were euthanized and the weight of collected tumors was determined. For biodistribution studies, the orthotopic 4T1 tumor-bearing BALB/c female mice were injected with Cy5-conjugated BSA $Cu(DDC)_2$ MONs *via* the tail vein. Then, *in vivo* imaging was conducted using an IVIS system (Caliper PerkinElmer, Hopkinton, USA) at predetermined time points. At the experimental endpoint, the mice were sacrificed, and the tumors and major organs were harvested for *ex vivo* imaging. The excitation wavelength was set at 640 nm, and the emission wavelength at 680 nm.

3. Results

3.1. Preparation and physicochemical characterization of $Cu(DDC)_2$ MONs

In our previous study, we developed SMILE technology to prepare $Cu(DDC)_2$ MONs with different amphiphilic molecules including methoxy poly(ethylene glycol) 5000 -*b*-poly(L-lactide) 5000 (PEG-PLA), TPGS, and 1, 2-distearoyl-sn-glycerol-3-phosphoethanolamine-poly(ethylene glycol) 2000 (DSPE-PEG). In the current study, BSA was explored as a stabilizer to prepare biomimetic $Cu(DDC)_2$ MONs with the same SMILE method. Of note, the decorated albumin can also serve as a targeting ligand to bind with albumin-binding proteins (*e.g.*, SPARC) that are overexpressed in the tumor cells [7,8,19–21]. When Cu^{2+} (a metal ion) was mixed DDC^- (an organic ligand), they formed insoluble $Cu(DDC)_2$ metal-organic complex. The DDC- and Cu^{2+} form complex at a mole ratio of 2:1 (Fig. 1A). BSA could effectively stabilize the *in situ* formed $Cu(DDC)_2$ MONs and prevent the formation of large aggregations. The formation of $Cu(DDC)_2$ was confirmed by the appearance of a specific peak at 435 nm. At the same time, a specific peak for DDC-Na at around 375 nm disappeared (Fig. 1C). The $Cu(DDC)_2$ MONs have a dark brown color which was due to the color of $Cu(DDC)_2$ complex, while both DDC- and Cu^{2+} were transparent without any obvious color (Fig. 1B). The formation of MONs was further confirmed by determining particle size with dynamic light scattering and TEM. The particle size of BSA $Cu(DDC)_2$ MONs was around 63 nm while the particle size of free BSA molecule was around 3 nm (Fig. 1E). Both of them have similar negative zeta potentials (Fig. 1D). The TEM results also confirmed the morphology and size of BSA $Cu(DDC)_2$ MONs, which was consistent with the particle size determined with the dynamic light scattering (Fig. 1F).

To optimize the formulation, we produced BSA $Cu(DDC)_2$ MONs with different BSA concentrations and theoretical drug concentrations. The yield and actual drug concentration of these MON formulations were determined (Fig. 2A & B, Tables S1 & S2). At the theoretical drug concentration of 0.5 mg/mL, we could successfully produce $Cu(DDC)_2$ MONs with BSA at the concentration from 0.1% to 4%. The yield was around 100% in all groups and actual drug concentration was around 0.5 mg/mL. At the theoretical drug concentration of 1 mg/mL, we could also successfully produce $Cu(DDC)_2$ MONs with BSA at the concentration from 0.5% to 4% with yield around 100% and actual drug concentration about 1 mg/mL. The yield was reduced to around 83% when the BSA concentration was 0.1%. At the theoretical drug concentration of 2 mg/mL, $Cu(DDC)_2$ MONs could be prepared at BSA concentration of 1%, 2%, and 4%, respectively. The yield was above 90% and actual drug concentration was around 2 mg/mL. The yield was reduced to 69% and 29% when BSA concentration was 0.1% and 0.5%. In summary, BSA is an excellent stabilizer for preparing $Cu(DDC)_2$ MONs. The yield was dependent on the concentration of BSA and $Cu(DDC)_2$. We could successfully prepare MONs at a wide range of $Cu(DDC)_2$ concentrations at high concentration of BSA. When the BSA concentration was low, we could only prepare MONs at low $Cu(DDC)_2$ concentrations. We also determined the particle sizes and PDI of $Cu(DDC)_2$ MONs prepared with different BSA concentrations and theoretical drug concentrations (Fig. S2 A & B, Table S3 &S4). We could successfully prepare $Cu(DDC)_2$ MONs with sizes less than 100 nm at most of the tested conditions. Both the $Cu(DDC)_2$ theoretical concentration and BSA concentration showed significant influence on particle size. When the theoretical drug concentration increased from 0.5 mg/mL to 2 mg/mL, the particle size increased accordingly at all groups with different BSA concentrations. At the theoretical drug concentration of 0.5 mg/mL, particle decreased with increased BSA concentration. At the theoretical drug concentration of 1 mg/mL or 2 mg/mL, the particle size decreased first and then slightly increased with the increase of BSA concentration. The smallest particle size of these two groups was achieved at BSA concentration of 1%. Based on these results, we decided to use theoretical drug concentration 2 mg/mL and 1% BSA as the condition to prepare BSA $Cu(DDC)_2$ MONs in our studies unless otherwise specified. The MONs will be prepared with DDC-Na solution [0.011 mmol/mL DDC-Na and 1% (w/v) BSA] and $CuCl_2$ solution [0.022 mmol/mL $CuCl_2$ and 1% (w/v) BSA].

The vortex mixing method is a convenient approach to produce $Cu(DDC)_2$ MONs at a small scale in the research laboratory. A large scale production method is needed for clinical translation or commercialization. Therefore, we developed a microfluidic device to prepare $Cu(DDC)_2$ MONs. This method could improve the mixing process and could be scaled up to produce MONs on a large scale. In this study, we used a microfluidic device to produce BSA $Cu(DDC)_2$ MONs (Fig. 3A). The microfluidic device was fabricated with a 3D printer. Our results showed that this microfluidic device could successfully produce MONs at the theoretical drug concentration of 2 mg/mL and 1% of BSA as the stabilizer. The effects of flow rate on BSA $Cu(DDC)_2$ MON drug concentration and particle size were investigated (Fig. 3B&C). The flow rate had a significant influence on final drug concentration and drug loading efficacy of $Cu(DDC)_2$ MONs. When the flow rate increased from 0.5 mL/min to 2 mL/min, the drug concentration in the MONs increased from 1.3 mg/mL to 1.9 mg/mL and the yield increased from 66% to 95%. The increase in flow rate might lead to a better mixing process, more efficient MON formation, and thus a higher drug concentration and yield. MONs prepared under different flow rate showed similar particle sizes (around 65 nm) and PDI values (around 0.2). At the optimized condition, $Cu(DDC)_2$ MONs prepared with the microfluidic device showed a similar drug concentration and particle size as those prepared with the vortex method with the same formulation. (*i.e.*, 1% BSA, 2 mg/mL $Cu(DDC)_2$ theoretical concentration). To further understand the mixing and MON formation process, a computational modeling approach was used to simulate this process. The simulation results also revealed the influence of flow-rate on $Cu(DDC)_2$ MON concentrations and demonstrated a good correlation with the experimental data (Fig. 3D). According to the simulation data, the concentration of $Cu(DDC)_2$ MONs increased with increased flow rate from 0.5 ml/min to 2 ml/min. Also, the concentration of MONs increased during the mixing process when the reaction mixture was moving forward in the channel of the microfluidic mixing device (Fig. 3D).

To predict the *in vivo* stability of $Cu(DDC)_2$ MONs, we incubated MON formulations with serum and determined the change of particle size. We tested the stability of three formulations: 1) the BSA/$Cu(DDC)_2$ MONs prepared with the vortex method, 2) the BSA/$Cu(DDC)_2$ MONs prepared with the microfluidic device, and 3) the TPGS/$Cu(DDC)_2$ MONs prepared with the vortex method (Fig. 4A). The BSA/$Cu(DDC)_2$ MONs showed almost no significant change in particle size during the incubation with serum for up to 57 h, indicating its excellent stability. In addition, the BSA/$Cu(DDC)_2$ MONs prepared with the vortexing method demonstrated a similar stability performance. In contrast, the TPGS/$Cu(DDC)_2$ MONs were less stable than the BSA/$Cu(DDC)_2$ MONs, showing a significant increase in particle size after 5 h of incubation.

The long-term storage stability of different MON formulations at the room temperature (25 °C) and in the refrigerator (4 °C) were also determined. When kept at the room temperature, a significant amount of precipitation was observed in the TPGS/$Cu(DDC)_2$ MON group and the drug concentration was also declined dramatically within one week. In contrast, the BSA/$Cu(DDC)_2$ MON groups showed excellent storage stability. No obvious precipitation or a significant decrease in drug concentration was observed for over 50 days (Fig. 4B). When stored at 4 °C, the BSA/$Cu(DDC)_2$ MON

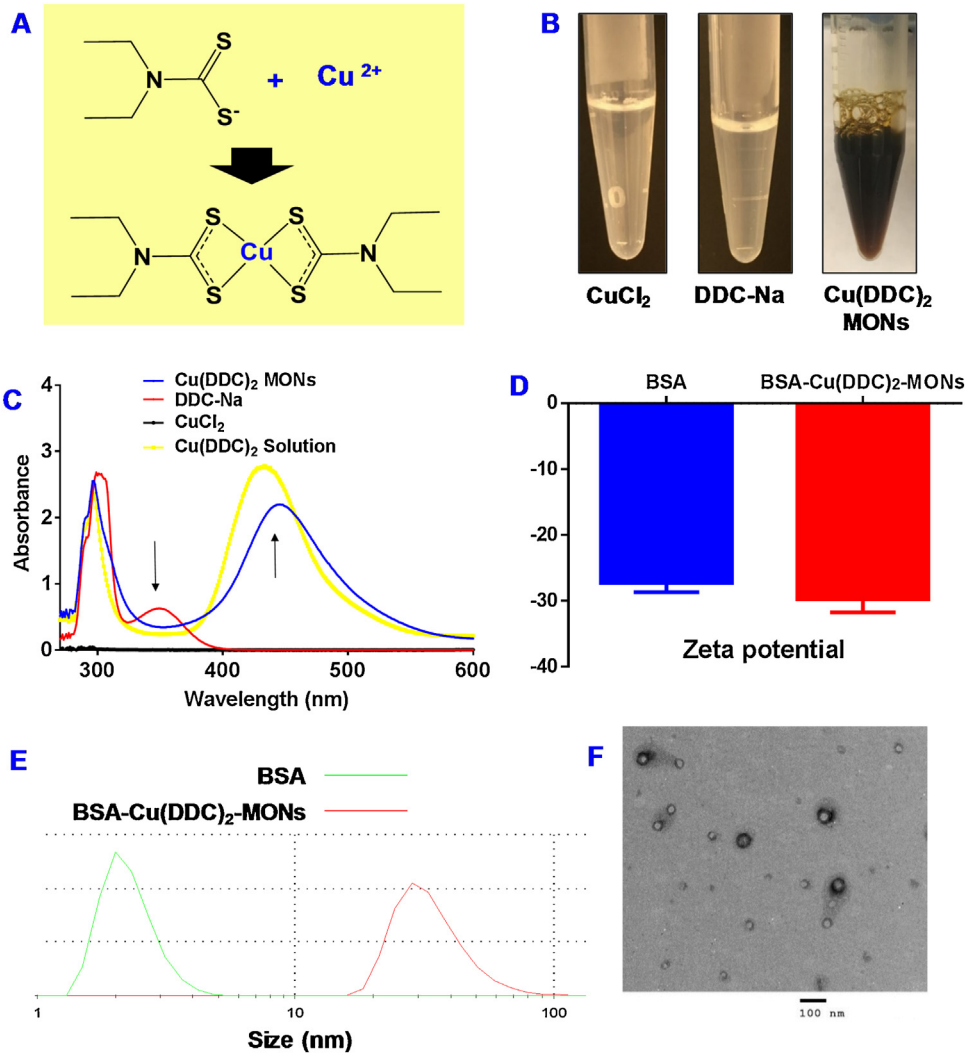

Fig. 1. Characterization of BSA Cu(DDC)$_2$ MONs. (**A**) Schematic illustration to show the Cu(DDC)$_2$ complex formation. (**B**) Photos of Cu(DDC)$_2$ MONs, DDC-Na and $CuCl_2$. (**C**) The spectrum of Cu(DDC)$_2$ solution, DDC-Na, $CuCl_2$, and Cu(DDC)$_2$ MONs. (**D**) Zeta potential. (**E**) Particle Size. (**F**) TEM of BSA Cu(DDC)$_2$ MONs.

groups also demonstrated good stability. Although the stability of the TPGS/Cu(DDC)$_2$ MON was improved at 4 °C, there was still a significant decrease in drug concentration during long-term storage (Fig. 4C).

3.2. Anticancer activity of Cu(DDC)$_2$ MONs

The anticancer activity of the BSA/Cu(DDC)$_2$ MONs were determined with the MTT Assay using two different breast cancer cell lines: MDA-MB-231 and 4T1(Fig. 5). Cells were treated with different formulations for 48 h before the MTT assay. For MDA-MB-231 cell, the IC_{50} of BSA/Cu(DDC)$_2$ MONs is 200 nM. In contrast, $CuCl_2$, DDC-Na monotherapy did not show significant toxicity on MDA-MB-231 cells at the tested concentrations (up to 1 μM). (Fig. 5). Similar anticancer efficacy was observed in 4T1 cells. The IC_{50} of the BSA/Cu(DDC)$_2$ MONs was 170 nM on 4T1 cells.

We also determined the viability of MDA-MB-231 and 4T1 cells treated with the BSA/Cu(DDC)$_2$ MONs using the Calcein AM and PI staining (Fig. 6). The portion of dead cells with red staining (PI) was higher at a higher drug concentration. Concurrently, the living cells with green fluorescence (Calcein AM) decreased with increased drug concentrations. We also observed that dose-dependent reduction in the number of attached cells due to the detachment of dead cells after the treatment. This is consistent with a previous report which indicated disulfiram/Cu induced cell detachment due to anoikis [22].

The anticancer efficacy was also tested with 3D-cultured 4T1 tumor spheroids. As shown in Fig. 7A, the majority of the cells of tumor spheroids were living cells with green staining when treated with $CuCl_2$ or DDC-Na. Tumor spheroids treated with BSA Cu(DDC)$_2$ MONs had less number of living cells and more dead cells. The viability of tumor spheroids was also determined with CellTiter-Blue reagents which showed similar results as demonstrated in the Calcein AM/PI staining experiment (Fig. 7B). Tumor spheroids treated with the BSA/Cu(DDC)$_2$ MONs showed significantly reduced cell viability. In contrast, the DDC-Na treated group showed a slight decrease in cell viability and $CuCl_2$ treated group showed almost no change of cell viability compared with the untreated control. The treatment of the BSA/Cu(DDC)$_2$ MONs also caused a significant change in tumor spheroids morphology (Fig. S3). Tumor spheroids treated with $CuCl_2$ or DDC-Na remained as intact round-shaped spheroids. In contrast, those treated with BSA/Cu(DDC)$_2$ MONs demonstrated compromised integrity with a large number of detached cells at the edge of spheroids.

We also tested the penetration ability of Cu(DDC)$_2$ MONs in tumor spheroids. The results showed that Cu(DDC)$_2$ MONs could penetrate the tumor spheroids and the penetration depth was around 30 μm (Fig. S5). The Cu(DDC)$_2$ drug release from pene-

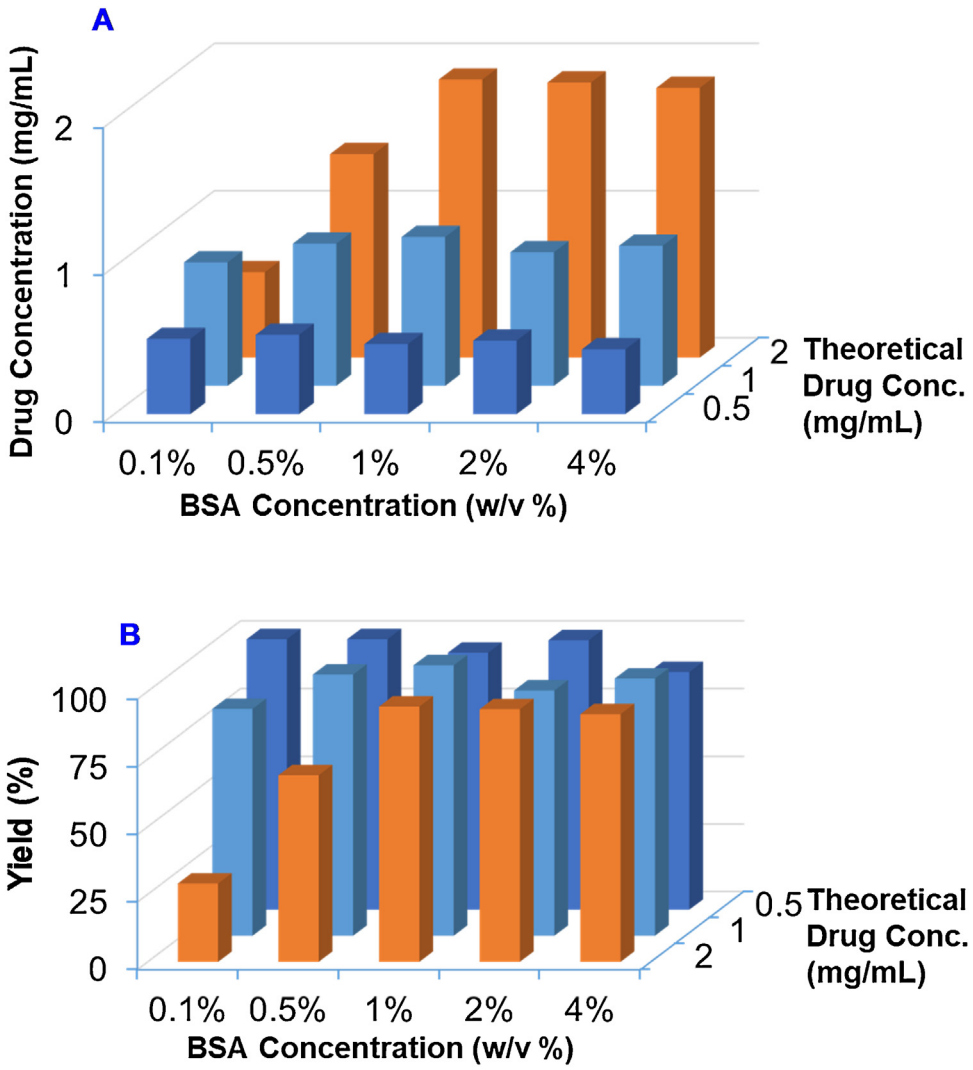

Fig. 2. Formulation optimization. The effects of BSA concentrations and theoretical drug concentrations on (**A**) drug concentration and (**B**) yield of BSA Cu(DDC)$_2$ MONs. Results are the mean (n = 3).

trated MONs could further diffuse into the tumor spheroids and kill additional neighboring tumor cells.

The would-healing study was performed to test the effects of the BSA/Cu(DDC)$_2$ MON on cell migration. Cell scratch was made on the 4T1 cell monolayer and then cells were treated with $CuCl_2$, DDC-Na, and the BSA/Cu(DDC)$_2$ MON (Fig. 8). $CuCl_2$ and DDC-Na did not have a significant effect on the cell migration towards the scratch and the gap was similar as observed in the untreated control group. BSA/Cu(DDC)$_2$ MONs significantly inhibited the cell migration and had a relatively large gap. Similar results were also observed in MDA-MB-231 cells (Fig. S4).

In vivo anticancer efficacy and biodistribution study was carried out in the orthotopic 4T1 breast tumor-bearing mice. Different formulations were administered through intravenous injection. The biodistribution results showed enhanced accumulation of MONs in the tumor region (Fig. 9). The accumulation of MONs in the tumor could be observed as early as 0.5 h post injection. The highest level was achieved around 8–12 h post injection. The signal was still detectable after 24 h. *Ex vivo* imaging also confirmed the accumulation of MONs in tumor regions. We also observed distribution of MONs in other organs such as liver, lung, and kidney at lower levels.

The treatment of the BSA/Cu(DDC)$_2$ MONs at a dose of 3 mg/kg resulted in significant inhibition of tumor growth (Fig. 10A), while no significant anticancer efficacy was observed in groups treated with BSA Cu(DDC)$_2$ (1.5 mg/kg), Cu(DDC)$_2$ solution (3 mg/kg), and equivalent dose of $CuCl_2$ solution, or DDC-Na solution. At the end of the study, tumors were collected and weighted (Fig. 10B&D). Among them, the BSA/Cu(DDC)$_2$ MON (3 mg/kg) group showed the most potent anticancer efficacy among all treatment groups. The body weight of tumor-bearing mice was also monitored continuously as an indication of acute systemic toxicity. The body weight of mice in all test group increased slightly during the course of *in vivo* experiment and no dramatic change of body weight was observed, indicating good tolerance of formulations (Fig. 10C).

4. Discussion

Multiple different methods were investigated in previous studies to prepare nanoscale metal-organic materials. These methods include solvo/hydrothermal synthesis, ultrasound-assisted synthesis, microwave-assisted synthesis, mechanochemical synthesis, reverse-phase emulsion, and liposome-based method [23]. In this work, we used a SMILE method and 3D-printed microfluidic device to prepare the BSA/Cu(DDC)$_2$ MONs as a novel formulation for DSF/Cu combination therapy. For this method, the nanoparticles were prepared by mixing Cu^{2+} (a metal ion) with DDC^- (a ligand) in aqueous solution in the presence of BSA stabilizer. According to a Lamer model, the MONs formation process includes two critical

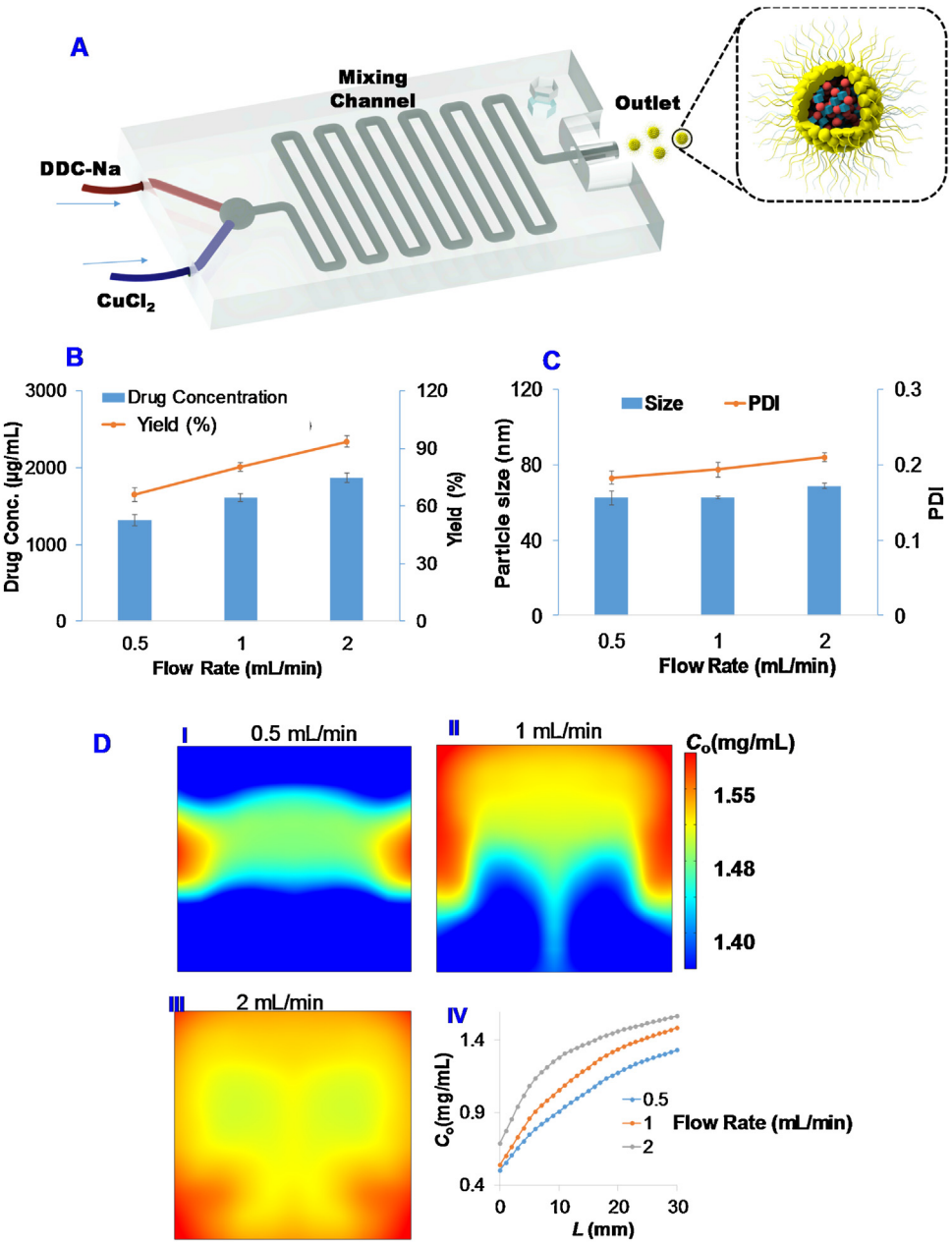

Fig. 3. Production of BSA Cu(DDC)$_2$ MONs with a microfluidic device. (**A**) Schematic illustration to show the preparation of BSA Cu(DDC)$_2$ MONs. The effects of flow rate on (**B**) drug concentration and yield, and (**C**) particle size and PDI. (**D**) Computational modeling to simulate the effect of flow rate on the MON formation. Cu(DDC)$_2$ concentration C_0 surface plot on the outlet cut cross plane for different flow rate (**I**) 0.5 mL/min, (**II**) 1 mL/min, and (**III**) 2 mL/min, respectively. (**IV**) The simulated Cu(DDC)$_2$ concentration C_0 *versus* the distance from mixing start point.

steps: (1) homogenous nucleation formation; and (2) termination of nucleation by rapid reduction of precursor concentration. The rapid nucleation process is critical for the synthesis of uniform NPs [24,25]. In the current study, the rapid mixing and reaction between Cu^{2+} and DDC^- is essential for the preparation of BSA Cu(DDC)$_2$ MONs.

In the current study, we designed a prototype 3D-printed microfluidic device to produce BSA-Cu(DDC)$_2$ MONs. It is a simple passive microfluidic mixing device with zigzag channels. The BSA-Cu(DDC)$_2$ MONs prepared with this device showed a small sub-100 nm nanoparticle size and had a narrow size distribution. The use of the microfluidic mixing device is an efficient method to achieve rapid and thorough mixing of samples [26]. The rapid mixing of Cu^{2+}, DDC^-, and BSA stabilizer in the mixing device contributed to the efficient production of Cu(DDC)$_2$ MONs. With the optimized condition, a high yield of MON production (95%) was achieved in the current study. The passive microfluidic mixing devices require no extra external energy. The mixing process relies mainly on chaotic advection effects or enhanced molecular diffusions. Besides the zigzag channel design used in the current study, there are multiple other passive microfluidic mixing devices which have 3-D serpentine structure, embedded barriers, or twisted channels. Furthermore, active mixing devices could also be used to enhance the mixing process by external forces such as acoustic/ultrasonic, dielectrophoretic, electrokinetic time-pulsed, electrohydrodynamic force, thermal actuation, magneto-hydrodynamic flow, and electrokinetic instability [26]. The microfluidic device used in the current study showed outstanding performance in the fabrication of BSA-Cu(DDC)$_2$ MONs. If needed, microfluidic mixing devices with sophisticated designs

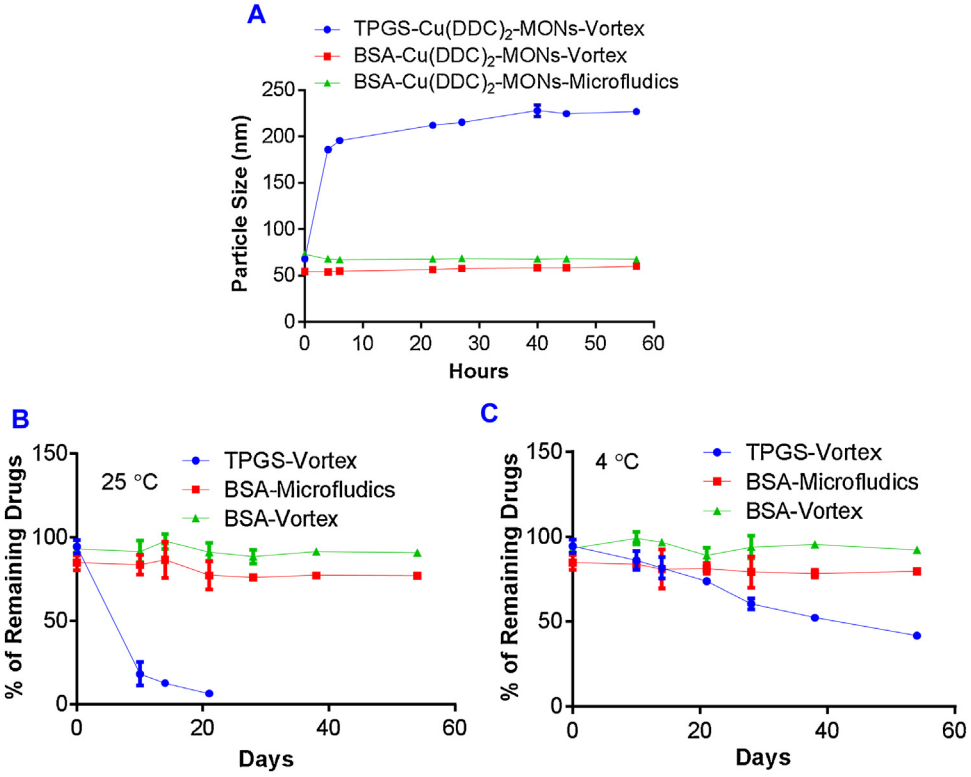

Fig. 4. Stability of Cu(DDC)$_2$ MONs. (**A**) MONs prepared with different methods were treated with 10% serum. Particle size was determined at different time points. Stability of Cu(DDC)$_2$ MONs at 25 °C (**B**) and 4 °C (**C**). Cu(DDC)$_2$ concentration was determined at different days. Results are the mean ± SD (n = 3).

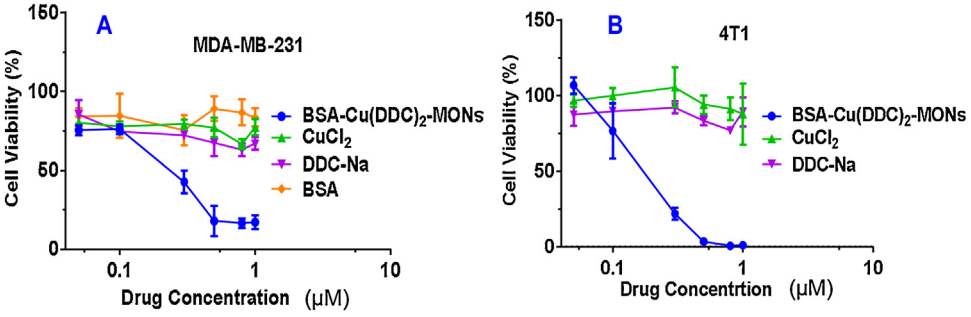

Fig. 5. MTT assay. (**A**) MDA-MB-231 and (**B**) 4T1 cells were treated with different formulations for 48 h and analyzed with the MTT assay. Results are the mean ± SD (n = 4).

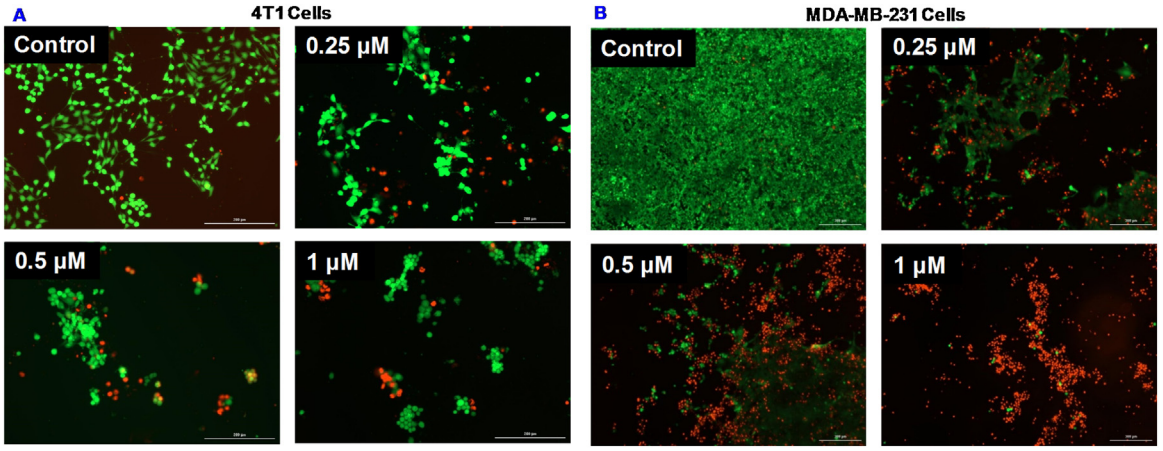

Fig. 6. Calcein-AM/PI staining. (**A**) 4T1 cells were treated with BSA Cu(DDC)$_2$ MONs for 18 h. (**B**) MDA-MB-231 were treated with BSA Cu(DDC)$_2$ MONs for 48 h. Then, cells were stained with Calcein-AM (green) and PI (red) at the end of drug treatment.

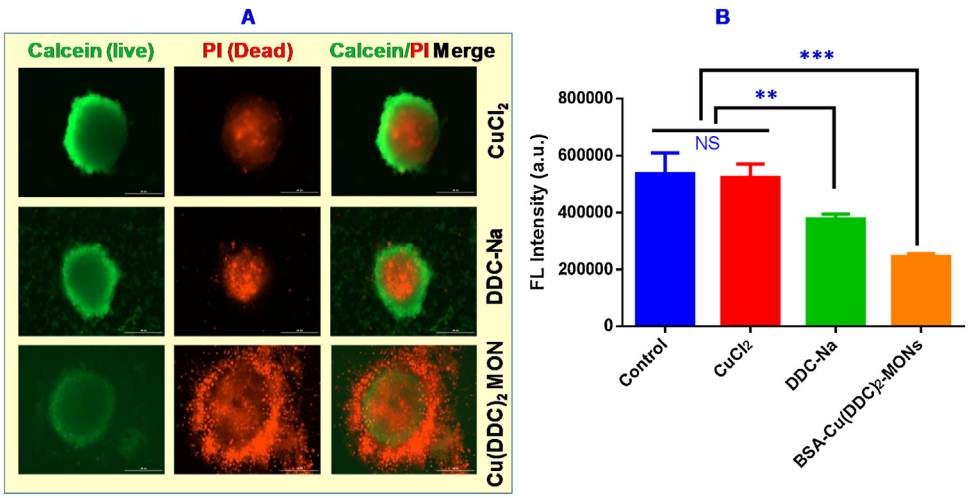

Fig. 7. Effects of BSA Cu(DDC)$_2$ MONs on 4T1 cell tumor spheroids. Tumor spheroids were treated with $CuCl_2$ (1 μM), DDC-Na (2 μM), and BSA Cu(DDC)$_2$ MONs (1 μM) for 72 h. At the end of treatment, tumor spheroids were analyzed with (**A**) Calcein-AM/PI staining, and (**B**) CellTiter-Blue Cell Viability Assay. Results are the mean ± SD (n = 3). ***, P < 0.001, and **, P < 0.01.

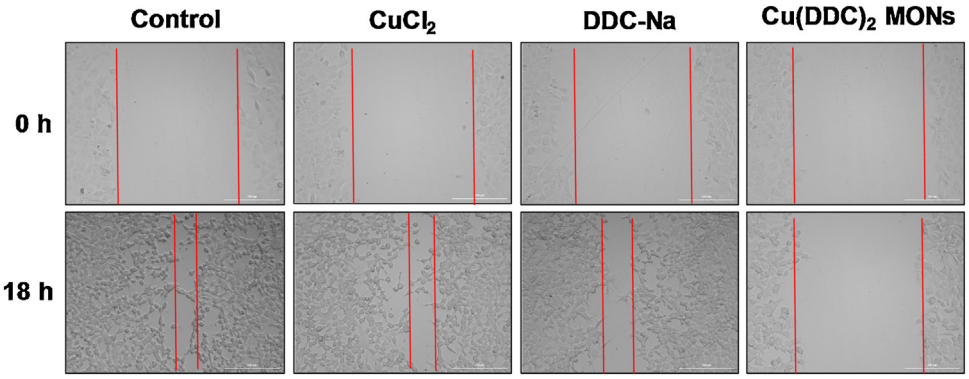

Fig. 8. Would-healing study. After generation of the scratch, 4T1 cells were treated with control, $CuCl_2$ (0.2 μM), DDC-Na (0.4 μM), and BSA Cu(DDC)2 MONs (0.2 μM) for 18 h. Photos were taken at 0 h and 18 h, respectively.

may be used to further improve the mixing process and the production of MONs.

The "vortexing method" is a convenient approach to prepare Cu(DDC)$_2$ MONs on a small scale. However, it will be challenging to produce a large amount of MONs with the "vortexing method". To address this challenge, we developed a microfluidic device- based method for scalable continuous production of MONs. The prototype device used in this study could produce 240 mL Cu(DDC)$_2$ MONs (2 mg/mL) per hour. This method is much more efficient than "vortexing method" which usually produces 1 mL Cu(DDC)$_2$ MONs per batch. The production efficiency of microfluidic device method could be further increased by adjusting the design of device. For example, multiple mixing units could be integrated into one single device and produce nanoparticles in parallel [27]. Because of the simple formulation and scale-up friendly preparation procedure, the use of microfluidic device for preparing Cu(DDC)$_2$ MONs will have a great potential for clinical translation and commercialization.

Inspired from nature, a biomimetic delivery system was developed utilizing components of biological systems to improve the drug delivery performance [18,28,29]. In this study, we selected BSA as a stabilizer which could stabilize Cu(DDC)$_2$ MONs and minimize the number of large aggregations. The amino acid residues of BSA (*e.g.,* Lys 199) could form coordination interactions with transition metal ions [30]. Therefore, BSA could effectively attach to the surface of Cu(DDC)$_2$ MONs through its strong interaction with Cu^{2+} and form a protective corona on the surface of MONs. This method has significantly enhanced the stability of Cu(DDC)$_2$ MONs. The biomimetic surface functionalization of MONs with BSA will also improve the *in vivo* biocompatibility.

Albumin-based biomimetic nanoparticle formulation also has great potential for tumor-targeted drug delivery. For example, Abraxane is a paclitaxel-albumin nanoparticle formulation approved by the FDA for chemotherapy. The albumin nanoparticle formulation could enhance drug delivery into tumors through the secreted protein acidic and rich in cysteine (SPARC) receptor [31]. SPARC is an albumin binding protein overexpressed in cancer cells and tumor vessel endothelial cells. The active recruitment of albumin by tumor microenvironment could be utilized as a method for tumor-targeted drug delivery. The biodistribution results showed enhanced accumulation of BSA Cu(DDC)$_2$ MONs in the tumor region (Fig. 9). The BSA-Cu(DDC)$_2$ MONs may target tumors through enhanced permeability and retention (EPR) effects and the secreted protein acidic and rich in cysteine (SPARC) receptor mediate cellular uptake [31]. We could further improve the tumor targeting and reduce the distribution in normal tissues and organs through functionalizing the surface of BSA-Cu(DDC)$_2$ MONs with additional tumor-targeting moieties. The albumin bears functional groups which could be used to conjugate tumor-targeting moieties [7,8]. We are in the process of functionalizing albumin with active tumor-targeting ligands which will further enhance the tumor-targeting and improve anticancer efficacy. The efficient intratumor penetra-

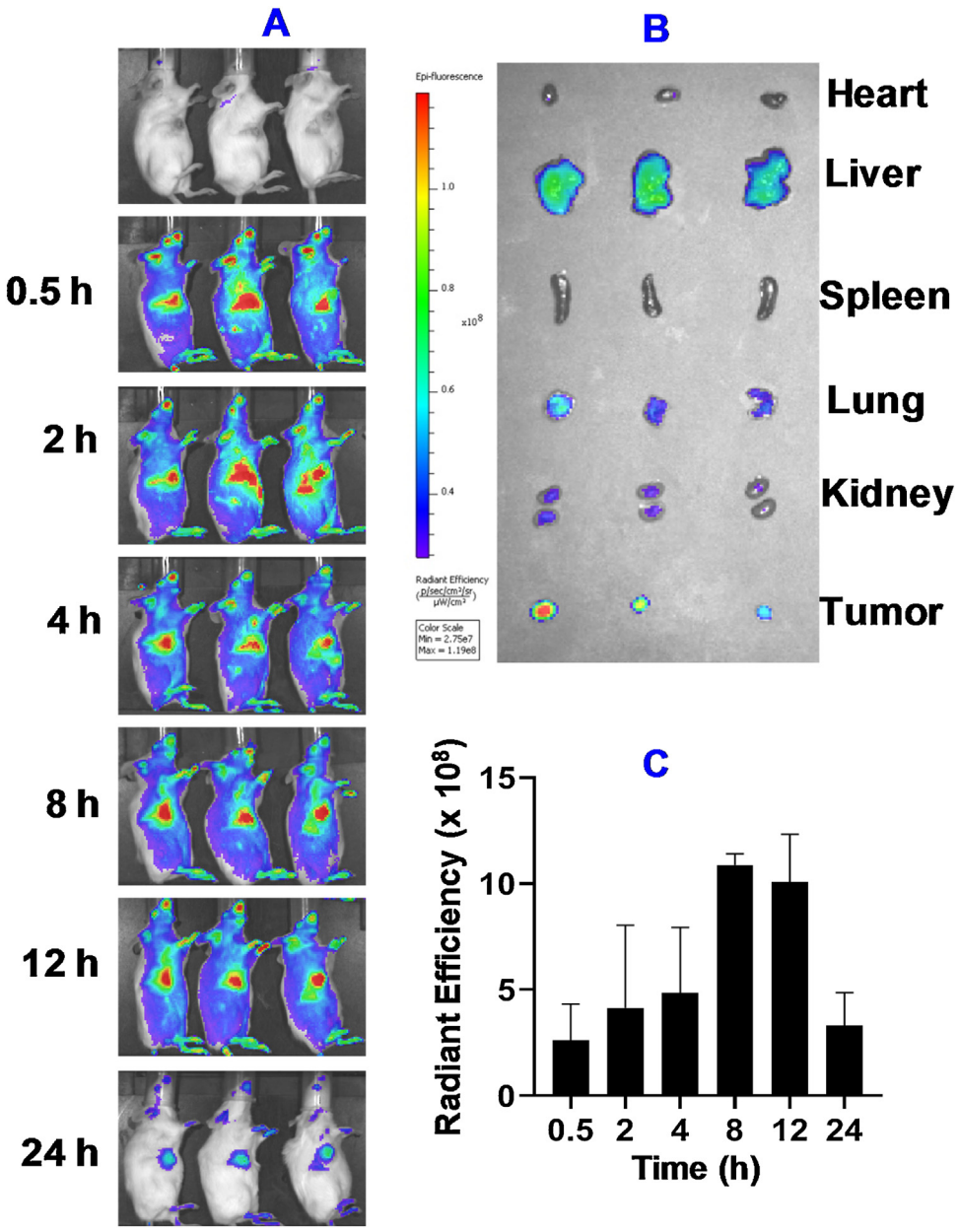

Fig. 9. ***In vivo*** biodistribution of Cy5-labeled BSA $Cu(DDC)_2$ MONs in mice with 4T1 orthotropic tumors determined with bioimaging. (**A**) The whole-body imaging at different time post injection. (**B**) *Ex vivo* imaging of isolated organs (heart, liver, spleen, lung, kidneys) and tumor. (**C**) The *in vivo* radiant efficiency of the tumor sites. Results are the mean ± SD (n = 3).

tion of nanoparticle are critical for their anticancer efficacy. We determined the penetration ability of BSA $Cu(DDC)_2$ MONs with *in vitro* tumor spheroids. Although the penetation depth was not deep enough reach the core of tumor spheroids, the $Cu(DDC)_2$ drugs released from penetrated MONs could further diffuse into the tumor spheroids and kill additional neighboring tumor cells. Also, we could further optimize the physicochemical properties of $Cu(DDC)_2$ MONs (*e.g.,* size, charge, and surface chemistry) or use other strategies to further enhance the penetration ability which will further improve the anticancer activities.

In this study, we used an *in vitro* wound healing study to determine the effects of drug treatment on cell migration which is a critical step for cell invasion and metastasis [22,32]. The effects of disulfiram (DSF) or DSF/Cu combination treatment on cell migration have been tested in several previous studies by wound healing study [22,33,34]. A recent study reported that the DSF/Cu treatment caused the down-regulation of focal adhesion kinase (FAK) [22]. The FAK is an important molecule of focal adhesion and associated with breast cancer metastasis [35]. Therefore, the $Cu(DDC)_2$ MONs which is nanoparticle formulation for DSF/Cu combination therapy might inhibit cell migration through the inhibition of FAK. Due to the clinical significance of tumor metastasis, it will be interesting to further explore the effects of BSA $Cu(DDC)_2$ MONs on the prevention of breast cancer metastasis with additional *in vitro* and *in vivo* studies. In the current study, we used a murine 4T1 tumor to test the *in vivo* anticancer efficacy. It is a widely used breast cancer model for testing the anticancer efficacy. However, the 4T1 tumor model is a very aggressive tumor model with rapid growth. The humane endpoint was reached in a relatively short period of time. Many other previous studies used 4T1 tumor model also showed short duration of study [36–38]. In the future, we will test BSA $Cu(DDC)_2$

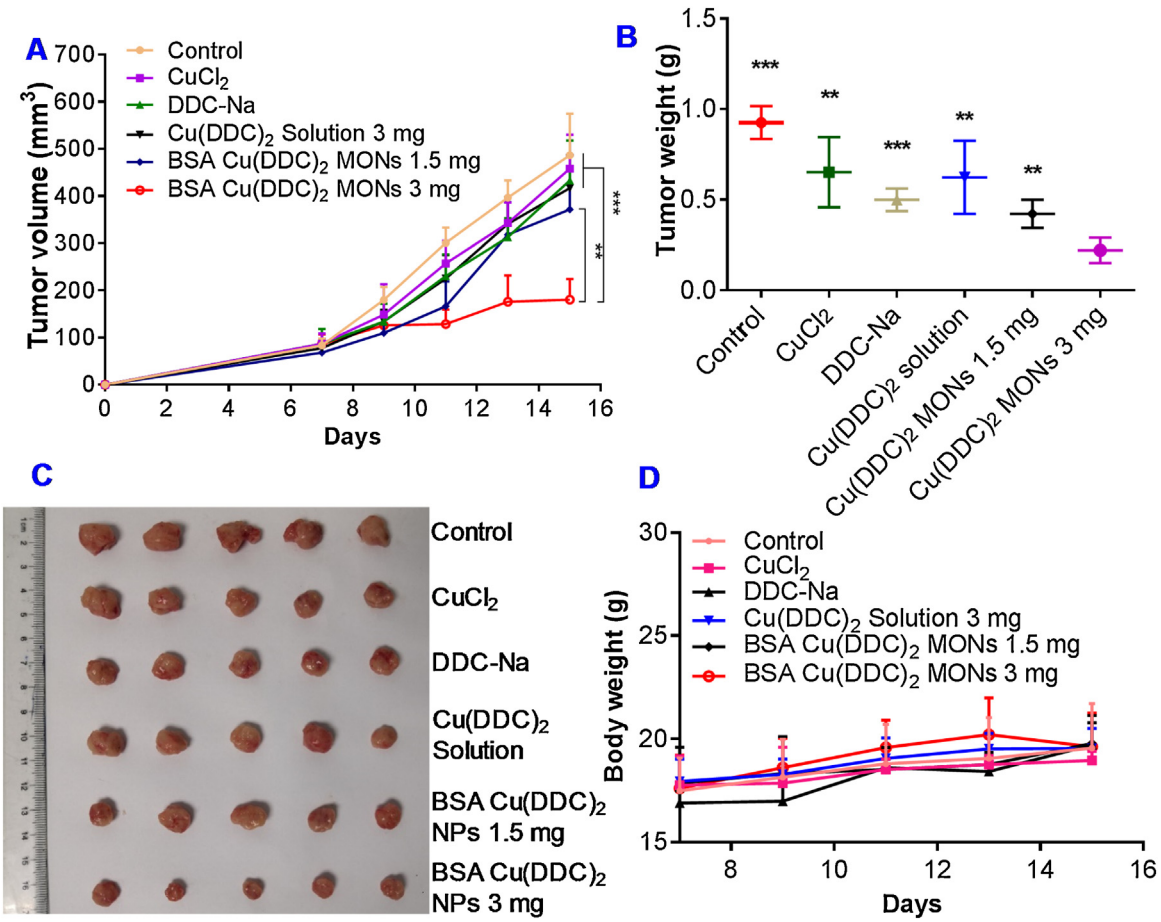

Fig. 10. ***In vivo*** anticancer studies. (**A**) Change of tumor volume in 4T1 tumor-bearing mice received intravenous injection of different formulation (**, $P < 0.01$, 3 mg/kg BSA $Cu(DDC)_2$ MONs *Vs* 1.5 mg/kg BSA $Cu(DDC)_2$ MONs; ***, $P < 0.001$, 3 mg/kg BSA $Cu(DDC)_2$ MONs *Vs* other groups). (**B**) Tumor weight measured at the end of the study (***, $P < 0.001$, **, $P < 0.01$, compared with 3 mg/kg BSA $Cu(DDC)_2$ MONs). (**C**) Photos of collected tumor tissues. (**D**) Change of body weight in 4T1 tumor-bearing mice during the course of study. Results are the mean ± SD (n = 5).

MONs in different tumor models which will allow us to observe long-term effects.

5. Conclusion

In conclusion, we designed a 3D-printed microfluidic device to prepare BSA $Cu(DDC)_2$ MONs with a SMILE technology developed in our lab. The optimized formulation has a small particle size (<100 nm) and narrow size distribution. The biomimetic MONs prepared with BSA as a stabilizer demonstrated excellent stability in serum and during long-term storage. The BSA $Cu(DDC)_2$ MONs demonstrated great potentials for treating breast cancers. To further develop the formulation, we will perform additional preclinical studies to extensively explore the *in vivo* pharmacokinetics, safety, and anticancer efficacies.

Declaration of Competing Interest

The authors declare no conflict of interest.

Acknowledgements

This project was supported by Auburn University start-up fund (F. Li), Launch Innovation Award (F, Li), and National Science Foundation Grant No. CBET-1701363 and National Institutes of HealthR35GM133795 (P. Chen). We are also thankful for the support of NFSC (81673382 and 81521005), the Strategic Priority Research Program of CAS (XDA12050307), and National Special Project for Significant New Drugs Development (2018ZX09711002-010-002) (Y. Huang).

Appendix A. Supplementary data

Supplementary material related to this article can be found, in the online version, at doi:https://doi.org/10.1016/j.apmt.2019.100492.

References

[1] L. Sleire, H.E. Førde, I.A. Netland, L. Leiss, B.S. Skeie, P.Ø. Enger, Drug repurposing in cancer, Pharmacol. Res. 124 (2017) 74–91.
[2] X. Lun, J.C. Wells, N. Grinshtein, J.C. King, X. Hao, N.-H. Dang, X. Wang, A. Aman, D. Uehling, A. Datti, J.L. Wrana, J.C. Easaw, A. Luchman, S. Weiss, J.G. Cairncross, D.R. Kaplan, S.M. Robbins, D.L. Senger, Disulfiram when combined with copper enhances the therapeutic effects of temozolomide for the treatment of glioblastoma, Clin. Cancer Res. 22 (2016) 3860–3875.
[3] Z. Skrott, M. Mistrik, K.K. Andersen, S. Friis, D. Majera, J. Gursky, T. Ozdian, J. Bartkova, Z. Turi, P. Moudry, M. Kraus, M. Michalova, J. Vaclavkova, P. Dzubak, I. Vrobel, P. Pouckova, J. Sedlacek, A. Miklovicova, A. Kutt, J. Li, J. Mattova, C. Driessen, Q.P. Dou, J. Olsen, M. Hajduch, B. Cvek, R.J. Deshaies, J. Bartek, Alcohol-abuse drug disulfiram targets cancer via p97 segregase adaptor NPL4, Nature 552 (2017) 194–199.
[4] A. Bruning, R.E. Kast, Oxidizing to death: disulfiram for cancer cell killing, Cell Cycle 13 (2014) 1513–1514.
[5] Z. Wang, J. Tan, C. McConville, V. Kannappan, P.E. Tawari, J. Brown, J. Ding, A.L. Armesilla, J.M. Irache, Q.B. Mei, Y. Tan, Y. Liu, W. Jiang, X.W. Bian, W. Wang, Poly lactic-co-glycolic acid controlled delivery of disulfiram to target liver cancer stem-like cells, Nanomedicine 13 (2017) 641–657.

[6] M. Wehbe, M. Anantha, M. Shi, A.W. Leung, W.H. Dragowska, L. Sanche, M.B. Bally, Development and optimization of an injectable formulation of copper diethyldithiocarbamate, an active anticancer agent, Int. J. Nanomed. 12 (2017) 4129–4146.
[7] P. Zhao, W. Yin, A. Wu, Y. Tang, J. Wang, Z. Pan, T. Lin, M. Zhang, B. Chen, Y. Duan, Y. Huang, Dual-targeting to cancer cells and M2 macrophages via biomimetic delivery of mannosylated albumin nanoparticles for drug-resistant cancer therapy, Adv. Funct. Mater. 27 (2017), 1700403.
[8] P. Zhao, Y. Wang, X. Kang, A. Wu, W. Yin, Y. Tang, J. Wang, M. Zhang, Y. Duan, Y. Huang, Dual-targeting biomimetic delivery for anti-glioma activity via remodeling the tumor microenvironment and directing macrophage-mediated immunotherapy, Chem. Sci. 9 (2018) 2674–2689.
[9] M. Wehbe, L. Chernov, K. Chen, M.B. Bally, PRCosomes: pretty reactive complexes formed in liposomes, J. Drug Target. 24 (2016) 787–796.
[10] W. Chen, W. Yang, P. Chen, Y. Huang, F. Li, Disulfiram copper nanoparticles prepared with a stabilized metal ion ligand complex method for treating drug-resistant prostate cancers, ACS Appl. Mater. Interfaces 10 (2018) 41118–41128.
[11] F. Li, C. Snow-Davis, C. Du, M.L. Bondarev, M.D. Saulsbury, S.O. Heyliger, Preparation and characterization of lipophilic doxorubicin pro-drug micelles, JoVE (2016), e54338.
[12] F. Li, M. Danquah, R.I. Mahato, Synthesis and characterization of amphiphilic lipopolymers for micellar drug delivery, Biomacromolecules 11 (2010) 2610–2620.
[13] W. Lu, F. Li, R.I. Mahato, Poly(ethylene glycol)-block-poly(2-methyl-2-benzoxycarbonyl-propylene carbonate) micelles for rapamycin delivery: in vitro characterization and biodistribution, J. Pharm. Sci. 100 (2011) 2418–2429.
[14] F. Li, Y. Lu, W. Li, D.D. Miller, R.I. Mahato, Synthesis, formulation and in vitro evaluation of a novel microtubule destabilizer, SMART-100, J. Control. Release 143 (2010) 151–158.
[15] H. Wang, F. Li, C. Du, H. Wang, R.I. Mahato, Y. Huang, Doxorubicin and lapatinib combination nanomedicine for treating resistant breast cancer, Mol. Pharm. 11 (2014) 2600–2611.
[16] Y. Chen, M. Zhang, H. Jin, Y. Tang, H. Wang, Q. Xu, Y. Li, F. Li, Y. Huang, Intein-mediated site-specific synthesis of tumor-targeting protein delivery system: turning PEG dilemma into prodrug-like feature, Biomaterials 116 (2017) 57–68.
[17] F. Li, M. Danquah, S. Singh, H. Wu, R.I. Mahato, Paclitaxel- and lapatinib-loaded lipopolymer micelles overcome multidrug resistance in prostate cancer, Drug Deliv. Transl. Res. 1 (2011) 420–428.
[18] Y. Chang, S. Yao, Y. Chen, J. Huang, A. Wu, M. Zhang, F. Xu, F. Li, Y. Huang, Genetically-engineered protein prodrug-like nanoconjugates for tumor-targeting biomimetic delivery via a SHEATH strategy, Nanoscale 11 (2019) 611–621.
[19] D. Li, M. Zhang, F. Xu, Y. Chen, B. Chen, Y. Chang, H. Zhong, H. Jin, Y. Huang, Biomimetic albumin-modified gold nanorods for photothermo-chemotherapy and macrophage polarization modulation, Acta Pharm. Sin. B 8 (2018) 74–84.
[20] P. Zhao, Y. Wang, A. Wu, Y. Rao, Y. Huang, Roles of albumin-binding proteins in cancer progression and biomimetic targeted drug delivery, ChemBioChem 19 (2018) 1796–1805.
[21] T. Lin, P. Zhao, Y. Jiang, Y. Tang, H. Jin, Z. Pan, H. He, V.C. Yang, Y. Huang, Blood–brain-barrier-penetrating albumin nanoparticles for biomimetic drug delivery via albumin-binding protein pathways for antiglioma therapy, ACS Nano 10 (2016) 9999–10012.
[22] J.Y. Kim, N. Lee, Y.-J. Kim, Y. Cho, H. An, E. Oh, T.-M. Cho, D. Sung, J.H. Seo, Disulfiram induces anoikis and suppresses lung colonization in triple-negative breast cancer via calpain activation, Cancer Lett. 386 (2017) 151–160.
[23] W. Cai, C.-C. Chu, G. Liu, Y.-X.J. Wáng, Metal–organic framework-based nanomedicine platforms for drug delivery and molecular imaging, Small 11 (2015) 4806–4822.
[24] V.K. LaMer, R.H. Dinegar, Theory, production and mechanism of formation of monodispersed hydrosols, J. Am. Chem. Soc. 72 (1950) 4847–4854.
[25] S. Wang, C.M. McGuirk, A. d'Aquino, J.A. Mason, C.A. Mirkin, Metal–organic framework nanoparticles, Adv. Mater. 30 (2018), 1800202.
[26] C.-Y. Lee, C.-L. Chang, Y.-N. Wang, L.-M. Fu, Microfluidic mixing: a review, Int. J. Mol. Sci. 12 (2011) 3263–3287.
[27] J.-M. Lim, N. Bertrand, P.M. Valencia, M. Rhee, R. Langer, S. Jon, O.C. Farokhzad, R. Karnik, Parallel microfluidic synthesis of size-tunable polymeric nanoparticles using 3D flow focusing towards in vivo study, Nanomedicine 10 (2014) 401–409.
[28] R. Li, Y. He, S. Zhang, J. Qin, J. Wang, Cell membrane-based nanoparticles: a new biomimetic platform for tumor diagnosis and treatment, Acta Pharm. Sin. B 8 (2018) 14–22.
[29] L. Wu, W. Chen, F. Li, B.R. Morrow, F. Garcia-Godoy, L. Hong, Sustained release of minocycline from minocycline-calcium-dextran sulfate complex microparticles for periodontitis treatment, J. Pharm. Sci. 107 (2018) 3134–3142.
[30] Y. Gou, Y. Zhang, Z. Zhang, J. Wang, Z. Zhou, H. Liang, F. Yang, Design of an anticancer copper(II) prodrug based on the Lys199 residue of the active targeting human serum albumin nanoparticle carrier, Mol. Pharm. 14 (2017) 1861–1873.
[31] D.A. Yardley, Nab-paclitaxel mechanisms of action and delivery, J. Control. Release 170 (2013) 365–372.
[32] J. Wang, J.S. Lee, D. Kim, L. Zhu, Exploration of zinc oxide nanoparticles as a multitarget and multifunctional anticancer nanomedicine, ACS Appl. Mater. Interfaces 9 (2017) 39971–39984.
[33] N.-n. Wang, L.-H. Wang, Y. Li, S.-Y. Fu, X. Xue, L.-N. Jia, X.-Z. Yuan, Y.-T. Wang, X. Tang, J.-Y. Yang, C.-F. Wu, Targeting ALDH2 with disulfiram/copper reverses the resistance of cancer cells to microtubule inhibitors, Exp. Cell Res. 362 (2018) 72–82.
[34] X. Duan, J. Xiao, Q. Yin, Z. Zhang, H. Yu, S. Mao, Y. Li, Multi-targeted inhibition of tumor growth and lung metastasis by redox-sensitive shell crosslinked micelles loading disulfiram, Nanotechnology 25 (2014), 125102.
[35] M. Luo, J.-L. Guan, Focal adhesion kinase: a prominent determinant in breast cancer initiation, progression and metastasis, Cancer Lett. 289 (2010) 127–139.
[36] Y. Wang, T. Yang, H. Ke, A. Zhu, Y. Wang, J. Wang, J. Shen, G. Liu, C. Chen, Y. Zhao, H. Chen, Smart albumin-biomineralized nanocomposites for multimodal imaging and photothermal tumor ablation, Adv. Mater. 27 (2015) 3874–3882.
[37] R. He, Y.-C. Wang, X. Wang, Z. Wang, G. Liu, W. Zhou, L. Wen, Q. Li, X. Wang, X. Chen, J. Zeng, J.G. Hou, Facile synthesis of pentacle gold–copper alloy nanocrystals and their plasmonic and catalytic properties, Nat. Commun. 5 (2014) 4327.
[38] L. Cheng, J. Liu, X. Gu, H. Gong, X. Shi, T. Liu, C. Wang, X. Wang, G. Liu, H. Xing, W. Bu, B. Sun, Z. Liu, PEGylated WS2 nanosheets as a multifunctional theranostic agent for in vivo dual-modal CT/photoacoustic imaging guided photothermal therapy, Adv. Mater. 26 (2014) 1886–1893.